Large scale finite element simulations of polycrystalline aggregates: applications to X-ray diffraction and imaging for fatigue metal behaviour

Henry Proudhon, Samuel Forest, Wolfgang Ludwig

LARGE SCALE FINITE ELEMENT SIMULATIONS OF POLYCRYSTALLINE AGGREGATES: APPLICATIONS TO X-RAY DIFFRACTION AND IMAGING FOR FATIGUE METAL BEHAVIOUR

H. Proudhon*, S. Forest* and W. Ludwig†,‡

* MINES ParisTech, Centre des matériaux, CNRS UMR 7633
BP 87, F-91003 Evry Cedex, France
† Université de Lyon, INSA-Lyon, MATEIS CNRS UMR 5510,
69621 Villeurbanne, France
‡ European Synchrotron Radiation Facility, BP220, 38043
Grenoble, France

ABSTRACT

Large scale finite element simulations of the elastoviscoplastic behaviour of polycrystalline aggregates have become a standard technique to study the stress-strain heterogeneities that develop in grains during deformation. For a long time, comparison between continuum crystal plasticity and experimental field measurements was confined to the observation of surface behaviour. As for example the study of the development of intense deformation bands at the free surface of a polycrystal. Recent 3D experimental techniques open new perspectives in computational crystal plasticity. After reviewing how to define a representative volume element for polycrystal properties and showing that actual 3D computations, including grain shapes and orientations, are really needed to accurately determine the stress and strains distributions, two examples of applications of large scale simulations are described in this paper.

First the simulation of 3D coherent X-ray diffraction in a polycrystalline gold sample is detailed. Based on the real geometry of the grains and their columnar nature, a 3D avatar is reconstructed. FE computations are then carried out to evaluate the effect of mechanical and thermal strain of the diffraction pattern resolved in the reciprocal space by complex FFT. Qualitative comparison with the experimental diffraction patterns shows that such computations can help understand the true nature of strain heterogeneities within the material.

The second example of application deals with short fatigue crack propagation in polycrystals. One fundamental problem caused by short fatigue cracks is that despite decades of research, so far no reliable prediction of the crack propagation rates, comparable to the well-known Paris law in the long crack regime, could be established. This “anomalous”

behaviour of short cracks is commonly attributed to factors like their complex three dimensional shapes and the influence of the local crystallographic environment affecting their propagation behaviour via a combination of physical mechanisms. Crystal plasticity computations based on the real grain shapes and orientations obtained thanks to diffraction contrast tomography are carried out using an ideal crack shape. The stress concentration at the crack tip is analysed with respect to possible crack growth directions.

1. INTRODUCTION

Continuum crystal plasticity has proved to be a powerful tool to interpret experimental results obtained in the deformation of metal polycrystals (Teodosiu, 1997). Large scale simulations on polycrystalline volume elements can now be performed with sufficient local discretization to predict the transgranular plastic strain fields. They are necessary for comparison with results of sophisticated 2D and 3D full field measurements providing total strain fields based on grid methods and/or image correlation techniques, lattice rotation fields by means of EBSD and, more recently elastic strain fields using for instance micro–diffraction techniques.

Even though continuum crystal plasticity constitutive equations do not account for the intricate dislocation mechanisms at work during plastic deformation, the continuum mechanical model gives relevant information about the strain heterogeneities induced in a polycrystal by the strong incompatibilities that develop at grain boundaries. These predictions are based on the precise kinematic description of the crystallographic nature of plastic slip in grains. For that purpose, full 3D simulations are necessary even when only 2D measurement information is available, due to the 3D nature of multislip mechanisms. The first illustrations of the tremendous heterogeneities that develop in polycrystals were provided in (Barbe et al., 2001a,b).

The drawback of standard continuum approaches is that they do not incorporate intrinsic length scales and cannot address satisfactorily size effects in plasticity. Most convincing validations of the approach were performed in the case of large grains. Advanced crystal plasticity models, based in particular on the description of both statistically stored and geometrically necessary dislocations, are now available to tackle grain size effects and strain fields at submicron scales (Forest, 2008). However they have not been used yet for quantitative comparisons due to the increased computational effort. They represent a link towards discrete dislocation dynamics approaches (Šiška et al., 2009).

However, precise confrontations between simulation and experiment are possible providing sufficient 3D information is available, especially 3D grain shape and orientation. This contribution addresses various aspects of computational polycrystal plasticity and its contribution towards the development and interpretation of new experimental 3D techniques based on X–ray diffraction and imaging. These methodologies are developed in particular for applications to fatigue behaviour of materials.

The first section tackles the problem of definition of representative volume element for polycrystal properties. This question is at the core of computational homogenization. The different levels of heterogeneities that develop in a material volume element are recalled. In the second section, we prove that the knowledge of the 3D shape and orientation of grains is required to assess the quality of numerical predictions even compared to 2D experimental field measurements. Cyclic plasticity is tackled in the case of the deformation of copper free–standing films, considering the evolution of strain heterogeneities close to grain bound-

aries during cycling. In the third section, computational crystal plasticity is applied to polycrystalline films under thermal loading. The heterogeneous displacement field is then used as input to predict coherent diffraction patterns which may be confronted to experimental measurements. Effects such as the grain shape and the strain level on the diffraction pattern are investigated. The last section deals with a promising field when crystal plasticity is coupled to real 3D microstructures obtained by diffraction contrast tomography. The prospect of simulating the presence of sharp interface such as cracks within the real grain network is demonstrated.

In the following, vectors are underlined and second and fourth rank tensors are boldface.

2. LARGE SCALE COMPUTATIONS OF POLYCRYSTALLINE AGGREGATES

2.1 RVE size for polycrystals. Computational homogenization methods are nowadays efficient tools to estimate effective properties of heterogeneous materials. They can take realistic distributions of phases and sophisticated constitutive equations of the constituents into account (Cailletaud et al., 2003). A key–point in such models is the determination of the appropriate size of volume elements of heterogeneous materials to be computed in order to get a precise enough estimation of effective properties. This is related to the long–standing problem of the determination of the size of the Representative Volume Element (RVE) in homogenization theory. It is known that RVE size is property and morphology dependent but a well–suited parameter is necessary for quantitative comparisons. Such a parameter was proposed in (Kanit et al., 2003).

In the present work, we illustrate this methodology to estimate the size of such a RVE in isotropic linear elastic copper polycrystals. The method has three main steps: the choice of a random model for polycrystalline microstructures containing a finite number of grains, the resolution of boundary value problems on such polycrystalline aggregates of increasing sizes and the analysis of the convergence of the calculated apparent properties towards an asymptotic value as a function of the number of grains and of the boundary conditions. The asymptotic value is regarded as the effective property. In other words, the objective is to find the minimum number of grains required in a volume element to estimate the effective elastic property with a given accuracy. The size of the RVE for several cubic elastic polycrystals was investigated in (Nygårds, 2003) using three–dimensional FE simulations and periodic boundary conditions.

Voronoi mosaics are used here as a random model to represent the polycrystalline morphology, as explained in (Kanit et al., 2003). For each realization, one given cubic volume V that contains a given number N_g of Voronoi cells is simulated. In the following, n realizations of volume V are considered. The number of cells for each realization of the microstructure obeys a Poisson distribution with given mean value $\bar{N}_g = N$. The mean volume of one Voronoi cell is equal to 1. No unit length is introduced because the models involved in this work cannot account for absolute size effects. As a result, one has $N = V$. This convention is used throughout the work. A crystal orientation is attributed to each Voronoi cell which is then regarded as an individual grain of the polycrystal. The crystallographic texture is assumed to be random. It is possible to impose a geometrical periodicity constraint at the boundary of the polycrystalline cube, as shown in figure 1.

The so–called multi–phase element technique is used in order to superimpose a regular 3D FE mesh on the Voronoi tessellation. The crystal orientation of the closest voxel is attributed to every integration point of each element of the mesh. The elements are 20–node quadratic

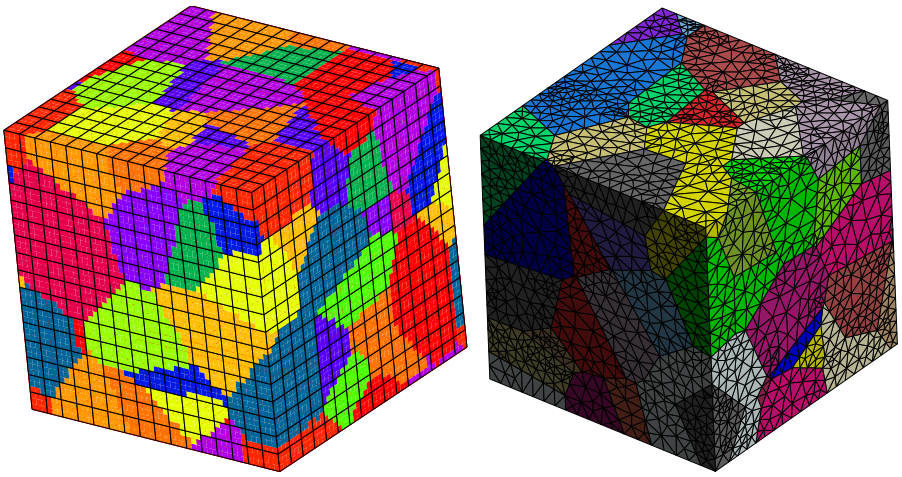

(a) Multiphase element technique (b) Conformal meshing of grain boundaries

Fig. 1: Meshing polycrystalline aggregates.

bricks with 27 Gauss points. A resolution of 16 elements per grain was satisfactory for the following calculations. Better suited mesh techniques are necessary to study the mechanical fields close to grain boundaries (figure 1b).

The largest volume computed in this section is a cube with $42^3 = 74088$ elements, i.e. 937443 degrees of freedom. Such computations are made possible in a reasonable time by using parallel computing. The FE program used in this work implements the subdomain decomposition method FETI* (Feyel, 1999). The mesh is split into 32 subdomains and the tasks are distributed on a platform of 32 processors (768 MB RAM, 800 MHz). Compatibility and equilibrium at interfaces between subdomains are restored by an iterative procedure. The whole resolution requires 21 GB of memory.

Three types of boundary conditions to be prescribed on an individual volume element V are considered (Sanchez-Palencia and Zaoui, 1987) :

- *Kinematic uniform boundary conditions* (KUBC) : The displacement vector $\underline{\boldsymbol{u}}$ is imposed at all points $\underline{\boldsymbol{x}}$ belonging to the boundary ∂V according to :

$$\underline{\boldsymbol{u}} = \boldsymbol{E}.\underline{\boldsymbol{x}} \quad \forall \underline{\boldsymbol{x}} \in \partial V \quad \Longrightarrow \quad <\boldsymbol{\varepsilon}> := \frac{1}{V}\int_V \boldsymbol{\varepsilon}\, dV = \boldsymbol{E} \tag{1}$$

  where $\boldsymbol{E}$ is a given constant symmetrical second–rank tensor. The macroscopic stress tensor $\boldsymbol{\Sigma}$ is then defined as the spatial average of the local stress tensor $\boldsymbol{\sigma}$.

- *Static uniform boundary conditions* (SUBC) : The traction vector is prescribed at the boundary ∂V according to :

$$\boldsymbol{\sigma}.\underline{\boldsymbol{n}} = \boldsymbol{\Sigma}.\underline{\boldsymbol{n}} \quad \forall \underline{\boldsymbol{x}} \in \partial V \quad \Longrightarrow \quad <\boldsymbol{\sigma}> := \frac{1}{V}\int_V \boldsymbol{\sigma}\, dV = \boldsymbol{\Sigma} \tag{2}$$

  where $\boldsymbol{\Sigma}$ is a given constant symmetrical second–rank tensor. The outer normal to ∂V at $\underline{\boldsymbol{x}}$ is denoted by $\underline{\boldsymbol{n}}$. The macroscopic strain tensor $\boldsymbol{E}$ is then defined as the spatial average of the local strain $\boldsymbol{\varepsilon}$.

*Mines ParisTech, ONERA, and NorthWest Numerics: Z-SeT/ZeBuLoN Finite Element Code, www.nwnumerics.com

- *Periodicity conditions* (PERIODIC) : The displacement field over the entire volume V takes the form

$$\underline{\boldsymbol{u}} = \boldsymbol{E}.\underline{\boldsymbol{x}} + \underline{\boldsymbol{v}} \quad \forall \underline{\boldsymbol{x}} \in V \tag{3}$$

  where the fluctuation $\underline{\boldsymbol{v}}$ is periodic. $\underline{\boldsymbol{v}}$ (resp. $\boldsymbol{\sigma}.\underline{\boldsymbol{n}}$) takes the same value (resp. opposite values) at two homologous points on opposite sides of V.

The local behaviour at every integration point inside each grain in the simulation is described by the fourth–rank linear elasticity tensor $\boldsymbol{c}$:

$$\boldsymbol{\sigma}(\underline{\boldsymbol{x}}) = \boldsymbol{c}(\underline{\boldsymbol{x}}) : \boldsymbol{\varepsilon}^e(\underline{\boldsymbol{x}}) \tag{4}$$

The partial differential equations to be solved using the FE method are the classical stress balance equations without body forces. For a given volume V, and owing to the linearity of the considered boundary value problems, fourth–rank tensors of apparent moduli $\boldsymbol{C}_E^{app}$ and apparent compliances $\boldsymbol{S}_\Sigma^{app}$ can be defined by the following macroscopic relations :

$$\boldsymbol{\Sigma} = <\boldsymbol{\sigma}> = \frac{1}{V}\int_V \boldsymbol{\sigma}\, dV = \boldsymbol{C}_E^{app} : \boldsymbol{E}, \quad \boldsymbol{E} = <\boldsymbol{\varepsilon}> = \frac{1}{V}\int_V \boldsymbol{\varepsilon}\, dV = \boldsymbol{S}_\Sigma^{app} : \boldsymbol{\Sigma} \tag{5}$$

The first relation is used for KUBC and PERIODIC problems, the second one for SUBC problems. Note that in general, the tensor $\boldsymbol{S}_\Sigma^{app}$ cannot be expected to coincide with the inverse of $\boldsymbol{C}_E^{app}$. However, for sufficiently large volumes V, the apparent moduli do not depend on the type of boundary conditions any longer and coincide with the effective properties of the medium:

$$\boldsymbol{S}_\Sigma^{app-1} = \boldsymbol{S}^{eff-1} = \boldsymbol{C}^{eff} = \boldsymbol{C}_E^{app} \tag{6}$$

For intermediate volumes V, the following inequalities, written in the sense of quadratic forms, hold (Huet, 1990) :

$$\boldsymbol{S}_\Sigma^{app-1} \leq \boldsymbol{C}^{eff} \leq \boldsymbol{C}_E^{app} \tag{7}$$

Shear loading conditions $\boldsymbol{E}_\mu$ and $\boldsymbol{\Sigma}_\mu$ are used in this work. The cubic elasticity constants of pure copper are taken from (Gairola and Kröner, 1981) :

$$C_{11} = 168400 \text{ MPa}, \quad C_{12} = 121400 \text{ MPa}, \quad C_{44} = 75390 \text{ MPa}$$

The corresponding value of the anisotropy coefficient $a = 2C_{44}/(C_{11} - C_{12})$ is 3.2.

Due to the uniform distribution of crystal orientations, the effective medium exhibits an isotropic linear elastic behaviour, described by effective bulk and shear moduli k^{eff} and μ^{eff}. For cubic symmetry, the apparent bulk modulus is not a random variable (Gairola and Kröner, 1981). It is uniquely determined from the single crystal elasticity constants according to the formula $k^{app} = k^{eff} = (C_{11} + 2C_{12})/3 = 137067$ MPa. As a result, the homogenization problem reduces to the estimation of apparent shear properties μ^{app} and *in fine* of the effective shear modulus μ^{eff}.

It is shown in (Kanit et al., 2003) that the fourth–rank tensor of apparent moduli $\boldsymbol{C}_E^{app}(V)$ obtained for a finite domain V containing N_g grains is generally not isotropic. However, its ensemble average $\bar{\boldsymbol{C}}_E^{app}(V)$, i.e. its mean value over a sufficiently large number of realizations turns out to be isotropic. This has been checked here for polycrystalline copper aggregates. The shear modulus associated with the isotropic elasticity tensor $\bar{\boldsymbol{C}}_E^{app}(V)$ coincides with $\bar{\mu}_E^{app}(V)$, the ensemble average of the apparent shear moduli $\mu_E^{app}(V)$ computed for a domain V of given size (or equivalently containing $N = V$ grains in average). Accordingly, the estimation of $\bar{\mu}_E^{app}(V)$ only requires the determination of $\mu_E^{app}(V)$ for each realization. This is the computation strategy adopted in this work. Similarly, using SUBC conditions, it is sufficient to compute μ_Σ^{app} for each realization.

The apparent shear moduli and compliances $\mu^{app}(V)$ were computed using volume elements V of increasing size, ranging from $V = 25$ to $V = 5000$ grains, with $n(V)$ realizations for every volume. Number n is chosen such that the estimation of the mean $\bar{\mu}^{app}(V)$ is obtained with a precision better than 1%. This precision is estimated according a simple sampling rule involving the standard deviation $D_\mu(V)$. Mean values and confidence intervals for the apparent shear modulus $[\bar{\mu}^{app}(V) - 2D_\mu(V), \bar{\mu}^{app}(V) + 2D_\mu(V)]$, are plotted in figure 2, as a function of volume size V. The mean apparent shear moduli strongly depend on the domain size and on the boundary conditions. However, the values converge towards an asymptotic constant as the volume size increases, as expected. A striking feature of these results is the very fast convergence of the periodic solution and, in contrast, the very slow convergence associated with homogeneous boundary conditions.

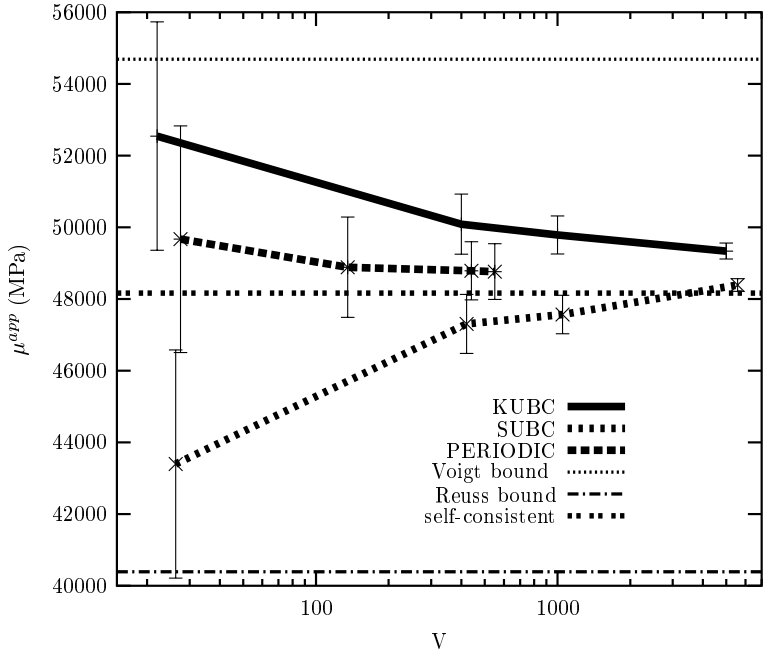

Fig. 2: Mean values and confidence intervals for the shear modulus μ^{app} as a function of domain size, for three different boundary conditions.

The computational homogenization methodology proposed in (Kanit et al., 2003) was applied to the determination of RVE sizes for the isotropic linear elastic behaviour of copper polycrystals. For a given precision of 1% in the estimation of the effective property, and a number of affordable computations ranging from 10 to 100, RVE sizes remain of the order of 40 to 400 grains, provided that periodicity boundary conditions are applied to the polycrystalline aggregates. The convergence of apparent properties obtained using homogeneous boundary conditions towards the effective modulus is significantly slower than for period-

icity conditions. The asymptotic shear modulus can be accurately estimated by a small number of huge computations or by a large number of small–scale computations, looking at the ensemble average of the apparent properties.

Finally, the calculated effective shear modulus can be compared with the self–consistent estimate according to (Gairola and Kröner, 1981). The self-consistent method predicts a shear modulus of 48167 MPa, which is 1.2% lower than the periodic solution found with 500 grains. This difference lies within the numerical precision associated with the mesh density chosen. Note that this result strongly depends on the anisotropy coefficient of the considered cubic material. The approach has also been applied to polycrystalline thin films in (El Houdaigui et al., 2007).

2.2 Prediction of strain heterogeneities in polycrystals. The previous methodology, including the specific boundary conditions, can be used to analyse the tremendous stress–strain heterogeneities that develop inside grains during deformation. In the case of anisotropic elasticity, grains boundaries are responsible for strong incompatibilities that are resolved by the development of high multiaxial stresses as show in (Zeghadi et al., 2007b). The case of crystal plasticity can still be accounted for by means of continuum mechanics and constitutive equations that take the crystallography of slip into account:

$$\boldsymbol{\varepsilon} = \boldsymbol{\varepsilon}^e + \boldsymbol{\varepsilon}^p, \quad \dot{\boldsymbol{\varepsilon}}^p = \sum_{s=1}^{N} \frac{\dot{\gamma}}{2} (\underline{\boldsymbol{m}}^s \otimes \underline{\boldsymbol{n}}^s + \underline{\boldsymbol{n}}^s \otimes \underline{\boldsymbol{m}}^s) \tag{8}$$

where the plastic strain $\boldsymbol{\varepsilon}^p$ is the sum of the slip γ^s on the N slip systems described by the slip direction $\underline{\boldsymbol{m}}^s$ and the normal to the slip plane $\underline{\boldsymbol{n}}^s$. Typical plastic flow rule is

$$\dot{\gamma}^s = \left\langle \frac{|\tau^s - x^s| - \tau_c}{K} \right\rangle^n \operatorname{sign}(\tau^s - x^s) \tag{9}$$

where $\tau^s = \boldsymbol{\sigma} : (\underline{\boldsymbol{m}}^s \otimes \underline{\boldsymbol{n}}^s)$ is the resolved shear stress. The critical resolved shear stress τ_c accounts for the hardening associated with statistically stored dislocations. We refer to reviews of specific constitutive equations for the evolution of dislocation densities like (Teodosiu, 1997). Note that kinematic hardening variable x^s must be included to account for cyclic plasticity.

The different levels of strain heterogeneities that develop in a polycrystal during straining are depicted in (Barbe et al., 2001b). The mean stress–strain curves for the whole volume can be compared to existing estimations based on homogenization models and especially variants of the self–consistent models. The mean stress–strain curves per grain or per grain orientation already show the heterogeneous nature of plastic deformation in polycrystals. The most striking result is the heterogeneity of plastic strain inside individual grains. Intense deformation bands tend to form crossing grain boundaries so that the grain unit is perhaps no longer the relevant entity to characterize the deformation processes (Barbe et al., 2009). The question of RVE size in plasticity for both the global and local material responses is still open due to the dependence of the results on the strain path to be applied to a volume element.

2.3 Grain boundary conditions and size–dependent properties of polycrystals. In such continuum crystal plasticity simulations, grain boundaries are treated as perfect or imperfect interfaces. At perfect interfaces, the displacement components are continuous and the trac-

tion forces are transmitted (Diard et al., 2005). Imperfect interfaces exist in the presence of intergranular damage or grain boundary sliding (Musienko and Cailletaud, 2009).

Continuum theories can still be applied to enrich the grain boundary behaviour and account, in a continuous way, for dislocation phenomena like pile–up formation at grain boundaries. This is the realm of strain gradient plasticity (Forest, 2008). Higher order continuity requirements, like continuity of plastic strain and transmission of higher order tractions mimic the development of internal stresses associated with geometrically necessary dislocations. For instance, the higher order couple stress tensor $\boldsymbol{M}$ conjugate to the dislocation density tensor, defined as the rotational of the plastic deformation tensor, leads to a an additional kinematic hardening component:

$$x = \mathrm{curl}\,\boldsymbol{M} = A\mathrm{curl}\,\mathrm{curl}\,(\gamma \underline{\boldsymbol{m}} \otimes \underline{\boldsymbol{n}}) = -A\Delta\gamma \tag{10}$$

in the case of single slip, where Δ is the Laplace operator and A a material parameter with unit MPa.mm^2. Such a formulation is akin to Aifantis original strain gradient plasticity model (Aifantis, 1987). This is how an intrinsic length scale arises in the generalized continuum model. Such enhanced crystal plasticity theories can be used to account for grain size effects in the response of polycrystalline aggregates, in the form of scaling laws close to Hall–Petch relationship.

3. SURFACE EFFECT AND THIN FILMS

3.1 Impact of 3D grain morphology on surface deformation. Validation of the continuum crystal plasticity model goes through the comparison of strain and lattice orientation fields with experimental field measurements. Those are most frequently available at the free surface of polycrystalline samples. That is why most convincing validations have been performed on multicrystalline samples containing a few grains or exhibiting a columnar microstructure (Teodosiu et al., 1993). Comparisons are much more difficult when the real shape of the grains below the free surface is unknown as it is the case for most EBSD and strain field measurements. In many contributions, a 2D finite element mesh is built from the 2D EBSD analysis. Then, an assumption of plane strain, or plane stress, or generalized plane strain, or 3D columnar grains is made (Héripré et al., 2007). Then, agreement between predicted and experimental fields usually remains only partial in the sense that strains and lattice rotation are correctly predicted for some grains but not for others.

To illustrate the impact of the 3D grain morphology on the surface strain, we have simulated virtual polycrystals with different grain morphologies but sharing the same surface shape as in figure 3a. The algorithm is explained in (Zeghadi et al., 2007b). The figure shows the free surface, normal to axis z, that is identical for two polycrystals and the underlying two layers of grains below the surface. A cut through the aggregate also shows the strongly different shapes and size of the grains in both cases. Simulations are such that the mean grain size is the same and the same crystal orientations are attributed to the corresponding grains cutting the free surface in both realizations. Then a tensile test has been simulated in direction y up to 1% overall tensile strain for an isotropic copper material. The equivalent plastic strain maps at the free surface are given in figure 3b. It appears that they strongly differ even though at some places, close to some grain boundaries, similar strain levels are reached. It is therefore impossible to validate a crystal plasticity model from the comparison of individual strain maps if the underlying morphology is unknown. However, statistical exploitation of the 2D information is still possible (Zeghadi et al., 2007a).

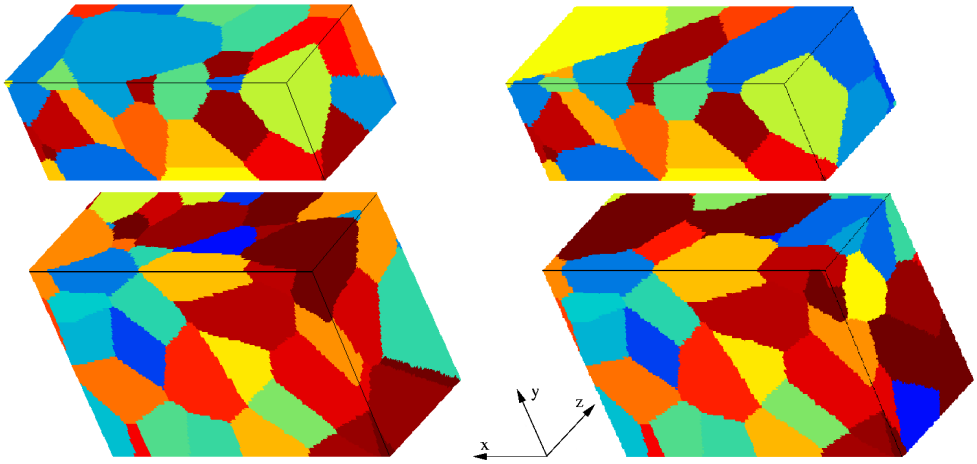

(a) Two realisations of polycrystalline aggregates with the same free surface grain morphology

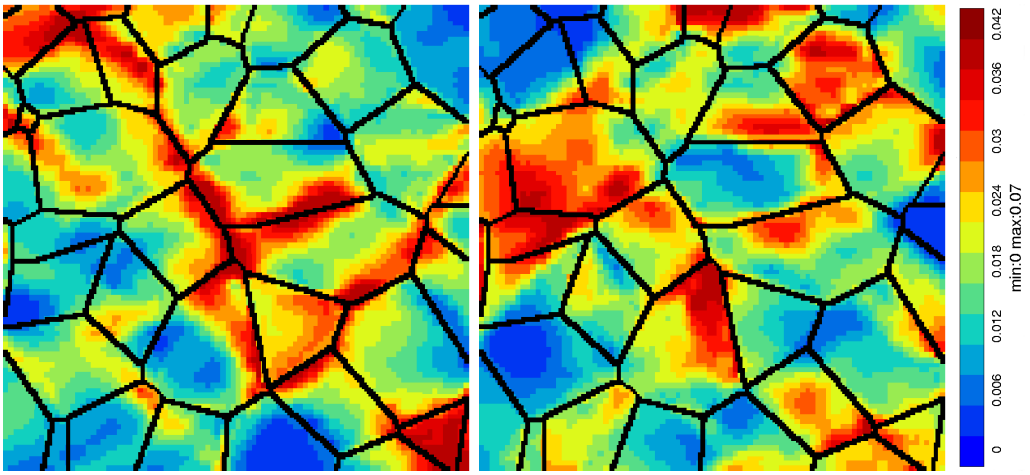

(b) Corresponding equivalent plastic strain field at the free surface after 1% overall tension

Fig. 3: Computed surface plastic strain after 1% tension, using two different polycrystalline microstructures exhibiting the same free surface grain morphology.

3.2 Cyclic plasticity of thin films. The cyclic behaviour of polycrystals can also be tackled by means of large scale simulations of polycrystalline aggregates. To reach sufficiently high number of cycles, the study can be limited to thin films with columnar microstructures, like the case of copper grains in figure 4 (top left). The orientations of grains in such thin films, typically of micron size, is mainly {111} with some {001} and random orientations (Šiška et al., 2007a). The analysis of plastic accommodation represents the first stage for the prediction of LCF crack initiation. We have analyzed both free–standing films and coatings on a rigid substrate (Šiška et al., 2007b). It was evidenced that, even though a limit cycle is reached after about 100 cycles in strain controlled cyclic tension (see figure 4 top right), the plastic strain fields at the free surface continues to evolve especially close to grain boundaries even after 1000 cycles. This is due to local ratchetting phenomena induced by the locally non symmetric stress cycles. Plastic strain fields turn out to be highly heterogeneous and form intense plastic bands crossing several grains (figure 4 bottom). However the presented simulations do not predict the formation of persistent slip bands and continuum modeling of such localization phenomena under cyclic loading conditions remains challenging (Flouriot et al., 2003). Probably stress–based loading conditions should be considered in the simulation. On the other hand, more specific dislocation mechanisms may well be

responsible for the formation of PSB finally leading to crack initiation (Déprés et al., 2004).

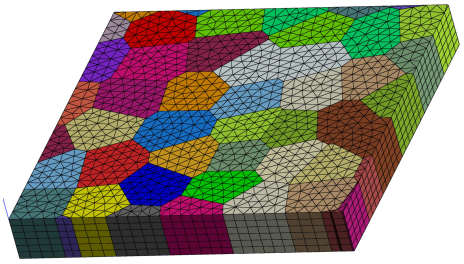

(a) Free–standing thin film made of columnar grains

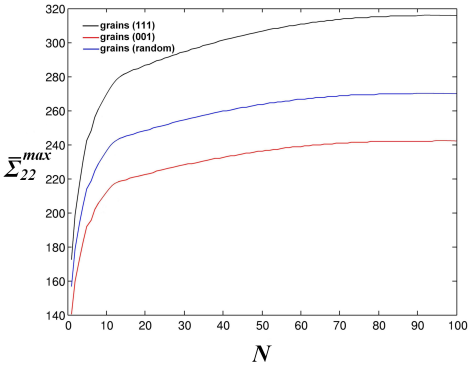

(b) mean stresses vs cycle number for a cyclic tension test

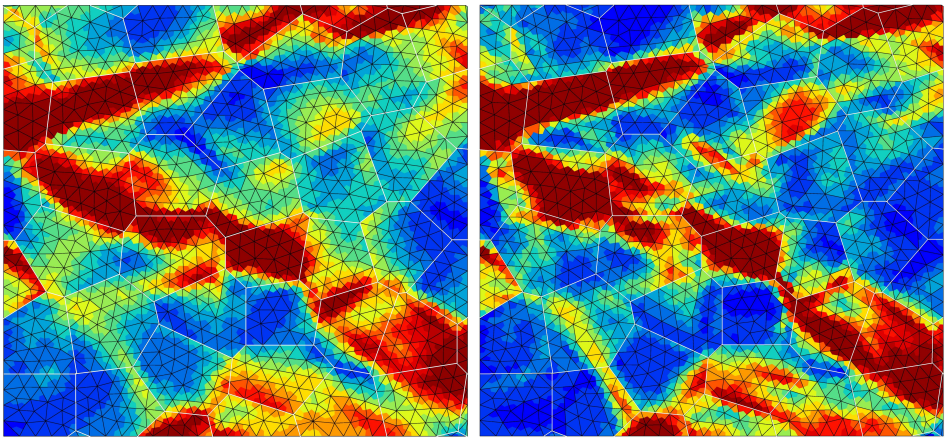

(c) plastic strain field at the first and 100th cycle

Fig. 4: Predictions of plastic strain development in a polycrystalline free–standing thin film under cyclic stress.

4. SIMULATION OF CXD PATTERNS

X–ray coherent diffraction has recently been recognized as a promising tool to experimentally characterize complex elastic strain fields in single crystals or grains in a polycrystal, up to very small length scales (Pfeifer et al., 2006; Vaxelaire et al., 2010). Such measurements can be performed on thin films, especially in polycrystalline films with columnar grains but the interpretation of experimental data has for now remained difficult and very limited.

While most attempts to analyse 3D coherent diffraction patterns turn to the inversion problem to retrieve the missing phase from the diffracted intensity, finite element simulations of the behaviour of polycrystalline aggregates have not been used to interpret diffraction patterns yet. The objective of the present section is to show that the detailed intragranular displacement field predicted by 3–dimensional FE computations can be exploited to delineate the respective effects of grain shape, orientation and strain on the evolution of complex diffraction patterns.

4.1 Theoretical aspects. Within the framework of the kinematic theory of diffraction[†], the

[†]this assumption is valid because of the small reflected intensity compared to incident beam (large rocking

3D intensity produced by a coherent beam diffracted by a small crystal is expressed as the sum of the complex amplitude scattered by each atom:

$$I(\underline{\boldsymbol{q}}) \propto \left| \sum_n f_n(\underline{\boldsymbol{q}}) \exp \imath \underline{\boldsymbol{q}}\, \underline{\boldsymbol{X_n}} \right|^2 \tag{11}$$

with $\underline{\boldsymbol{X_n}}$ being the atomic position at n and f_n its scattering factor.

For a deformed crystal, we define $\underline{\boldsymbol{u}}(\underline{\boldsymbol{X}})$ as the displacement vector field which is the difference between the current and initial atom positions. The displacement field can be easily introduced and Eq. 11 which can be rewritten using a Fourier transform, within Takagi approximation (Takagi, 1969) and with $\underline{\boldsymbol{q}} \simeq \underline{\boldsymbol{G}}$:

$$I(\underline{\boldsymbol{q}}) \propto \left| TF\left\{\rho(\underline{\boldsymbol{X}}).\exp\left(\imath \underline{\boldsymbol{G}}.\underline{\boldsymbol{u}}(\underline{\boldsymbol{X}})\right)\right\} \right|^2 \tag{12}$$

The diffracted intensity $I(\underline{\boldsymbol{q}})$ can therefore be evaluated using the displacement field computed by large scale finite element analysis of a polycrystal sample.

4.2 Numerical simulation of a 3D coherent diffraction pattern. To compute the strain heterogeneities within a polycrystalline sample, a suitable mesh of the grains must be obtained. A standard way to mesh a polycrystal is to use Voronoi tessellations in two or three dimensions as shown in sections 2.1 and 3.1, but real grain geometry can also be used favourably if available (Parisot et al., 2001). In this work, thanks to their columnar nature, the precise shape of the grains can be extracted from a SEM image in back scattered electron mode (which provides some crystalline contrast), as shown on Fig. 5. The resulting 2D microstructure is then extended in the Z direction to obtain the 3D mesh with 133 grains. The mesh closely matches the gold sample size of $10 \times 10 \times 0.2$ µm. As the exact orientations of the grains were not available at the time of the computations, a fiber texture with $\langle 111 \rangle$ parallel to the surface and random in-plane orientation, is applied. To match as closely as possible the experimental orientation set, small deviations of the $\langle 111 \rangle$ direction are taken into account. These deviations are applied randomly within the experimental scatter, as measured on the laboratory X-ray diffractometer.

FEM calculations were performed using Z-SeT software suite[‡] using linear elasticity behaviour with cubic anisotropy to represent the gold crystal network. The following elastic constants C_{ij} have been used (Neighbours and Alers, 1958): $C_{11} = 192\,340$ MPa, $C_{12} = 163\,140$ MPa and $C_{44} = 41\,950$ MPa. For FCC crystals, the Bragg vector is $\underline{\boldsymbol{G_{hkl}}} = \frac{2\pi}{a}[h,k,l]$ with $a = 0.4078$ nm the atomic spacing. The effect of temperature on these parameters is neglected.

The different steps chained to obtain the 3D diffraction pattern on a selected grain are shown on Fig. 6. Starting with the 3D mesh and the grain orientation set (Fig. 6a), boundary conditions are applied (sample fixed on the lower face to simulate a rigid glass substrate and a temperature change of $\Delta T = 100K$ applied linearly over time, Fig. 6b). FEM calculation is carried out to retrieve the heterogeneous stress and strain fields (Fig. 6c). The displacement field $\underline{\boldsymbol{u}}(\underline{\boldsymbol{X}})$ is then transferred onto a regular mesh (typically $200 \times 200 \times 5$ elements,

curve ($\simeq 0.3°$))

[‡]available from www.nwnumerics.com

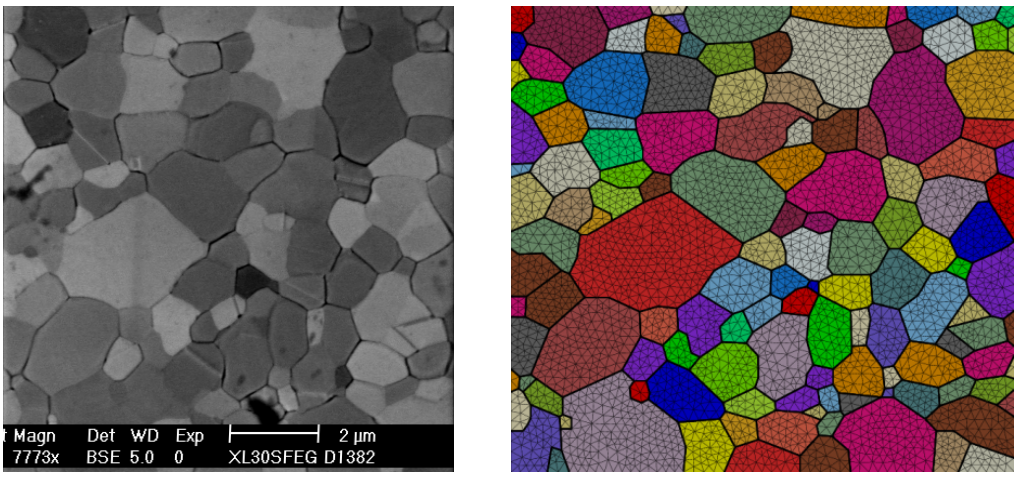

(a) SEM image of isolated polycrystal

(b) Grain topology extracted from the SEM image

Fig. 5: Extraction of the surface grain topology.

Fig. 6d). Finally Eq. 12 is computed with a complex FFT[§] on a 200^3 array filled with zero outside the grain and with $\{\cos(2\pi/a(hu_x + ku_y + lu_z)), \sin(2\pi/a(hu_x + ku_y + lu_z))\}$ inside the selected grain. The amplitude of the complex output is stored into a 3D data set which can then be visualised in the reciprocal space (q_x, q_y, q_z) and further analysed (Fig. 6e).

4.3 Application to a selected grain. The numerical diffraction procedure has been used with a particular grain named grain#52 in the following and results are presented on Fig. 7. First column, no deformation has been applied yet so that the diffraction pattern shows the effect of the shape only. One can see a symmetric pattern (DFT with a real input). Subsequent thermal straining clearly introduces some strain heterogeneities (see von Mises stress contours) and the diffraction pattern deforms and progressively loses its symmetry.

It should be noted that those computations were carried out using the full displacement field to represent the elastic stretch and rotation of the local crystal lattice. When the sample deforms elastically, the full displacement field can indeed be used to simulate CXD patterns but this becomes less and less valid anymore as soon as plasticity develops within the considered grains. The idea behind this is that the glide of dislocations through the element do not distort nor rotate the lattice. To predict diffraction patterns in the plastic regime, it is then possible to use an approximate elastic field, based on a first order Taylor expansion of the deformation field near the center of the grain. Using such a field may lead to more realistic CXD patterns when considering plastic deformation of those samples.

By simulating the heterogeneous displacement field in a polycrystal, one can easily change a variety of parameters like grain shape and/or orientation, level of strain, boundary conditions... Tying those computations with FFT can provide a very useful tool to understand the complexity of the real 3D coherent diffraction pattern observed experimentally.

[§]Computations based on FFTW version 3.2.1(Frigo and Johnson, 2005)

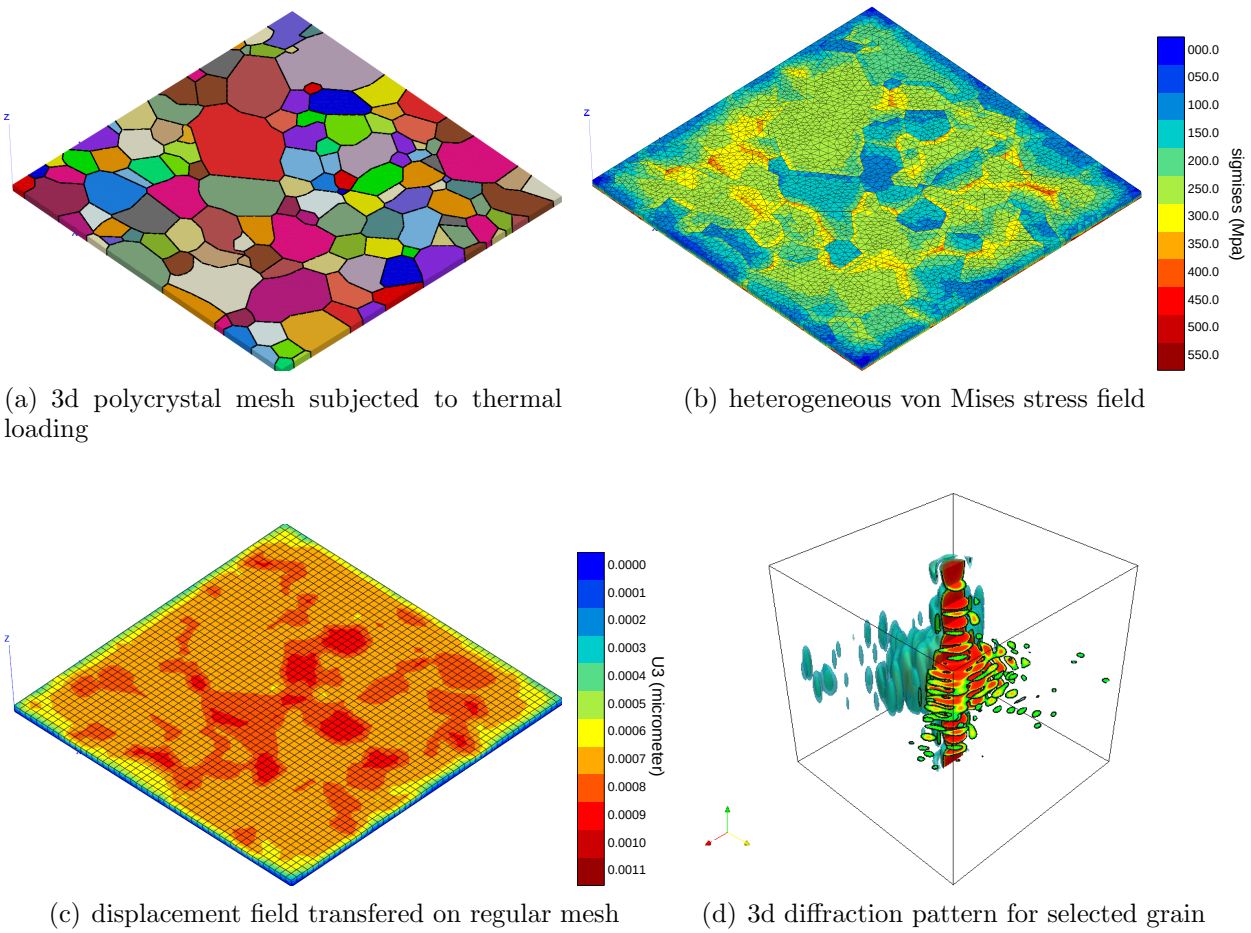

(a) 3d polycrystal mesh subjected to thermal loading

(b) heterogeneous von Mises stress field

(c) displacement field transfered on regular mesh

(d) 3d diffraction pattern for selected grain

Fig. 6: Illustration of the methodology used to compute the 3d diffraction pattern on a selected grain within a polycrystalline microstructure.

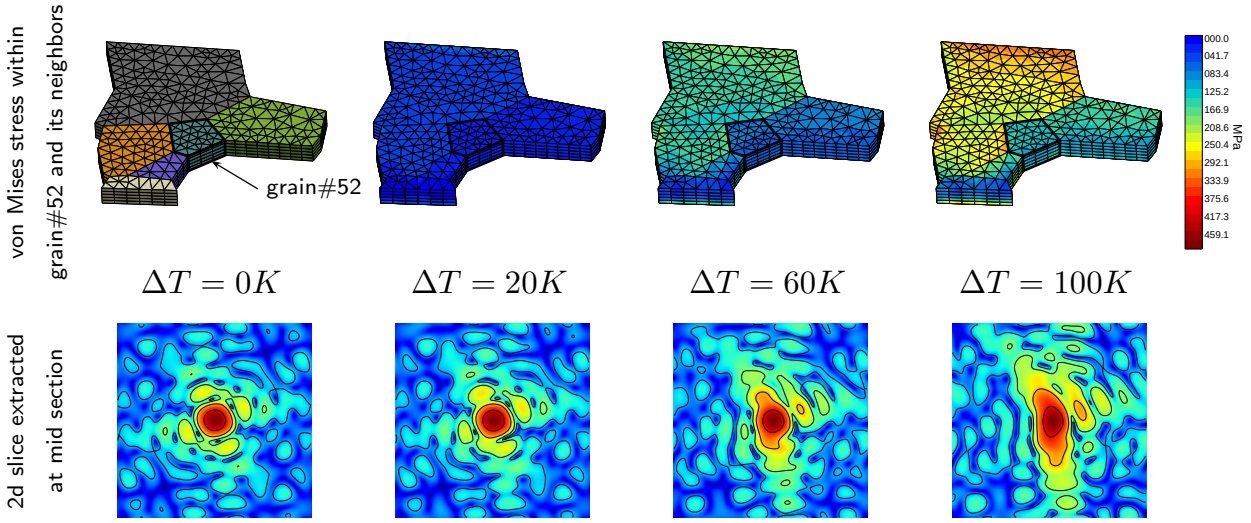

Fig. 7: Simulation of coherent diffraction in grain#52 at different strain levels; top line depicts the heterogeneous von Mises stress field in grain#52 and some of its neighbours, bottom line shows slices extracted from the diffraction pattern at $q_z = 0$.

5. FEM BASED ON DCT EXPERIMENTS

DCT is a monochromatic beam rotation technique, combining the principles of 3D X-ray diffraction microscopy (Poulsen, 2004) and X-ray micro tomography. During a 360 degree

continuous rotation of the sample, each grain runs through a series of diffraction alignments, giving rise to diffracted beams. Part of these diffraction spots are captured on the high resolution imaging detector system, positioned closely behind the sample (see Fig. 8). Like in conventional micro tomography, one can determine the three-dimensional distribution of the X-ray attenuation coefficient from the attenuation in the transmitted beam.

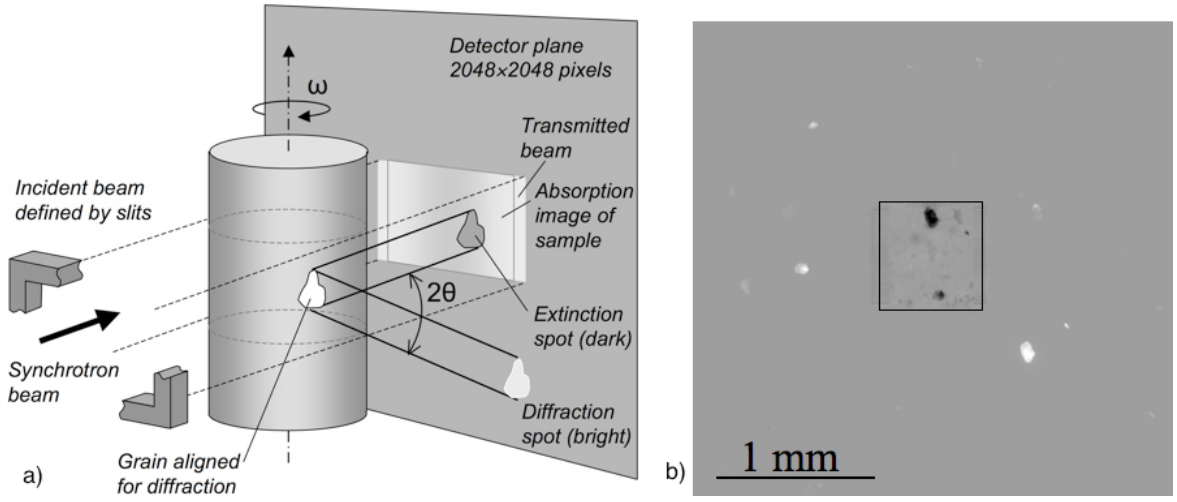

Fig. 8: DCT shares a common setup with X-ray microtomography. The transmitted as well as (part of the) diffracted beams are captured on the high resolution detector positioned closely behind the sample.

The analysis of the diffracted beams provides access to the crystalline microstructure. The processing route is summarized in Fig. 9. After segmentation, Friedel pairs of diffraction spots (hkl and -h-k-l reflection from the same grain) are automatically identified ("pair matching"). A polycrystal indexing algorithm based on the analysis of such pairs of diffraction spots (Ludwig et al., 2009b) classifies the diffraction spots according to their grain of origin and determines the average orientation and elastic strain state of the grains.

The 3D shape and the position of the grains in the sample volume are determined with the help of algebraic reconstruction techniques, using the 2D diffraction spots as parallel projections of the unknown 3D grain volume (see Fig. 9, bottom right).

Thanks to those recent advances with X-ray microtomography, the complete set of grain shapes and orientations in a polycrystalline microstructure can no be obtained (Ludwig et al., 2009a). From there, it becomes possible to recreate a numerical avatar of the specimen for computational purposes. This can be done by first meshing all the grain boundaries with shell elements. This interface mesh can then be used as input for a generalised 3D mesher (eg. tetgen/GHS3D software package) to obtain a full 3D mesh suitable for FEM computations. This process is demonstrated in Fig. 10 using a dataset reconstructed from a cylindrical sample of 600 µm diameter made of large grain β titanium alloy.

The study of short fatigue cracks is a domain where 3D in situ microtomography can bring a lot of new insight, especially if experiments and simulations can be carried out in synergy. Here experiments are still far ahead computations since based on previous work using attenuation and phase contrast (Ferrié et al., 2006) and new possibilities offered by diffraction contrast, it may now be possible to follow a small crack within a set of grains during its growth. One problem with computation accounting at the same time for a grain network

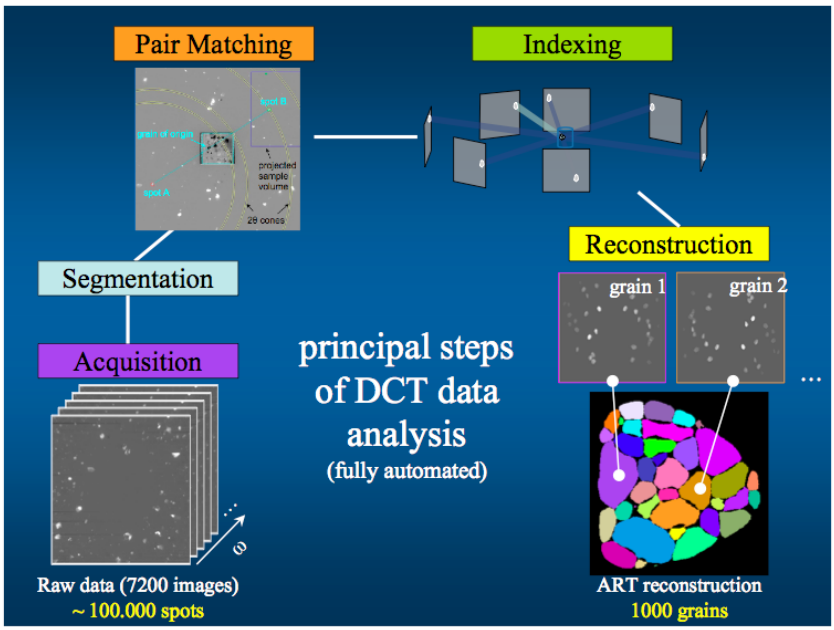

Fig. 9: Principal steps of the DCT analysis procedure.

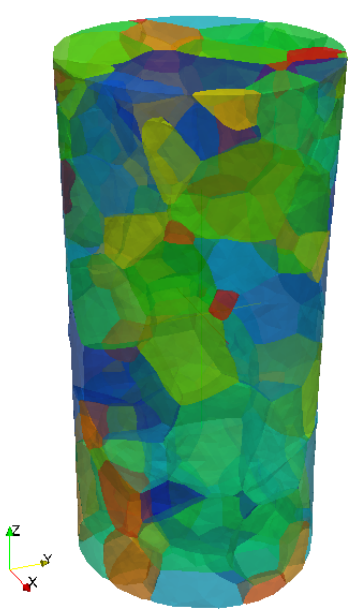

(a) Grains from DCT experiment (grains have been made half transparent)

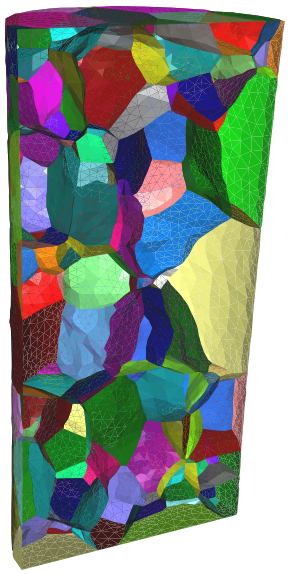

(b) Grain boundaries meshed with shell elements (only half of the sample is shown)

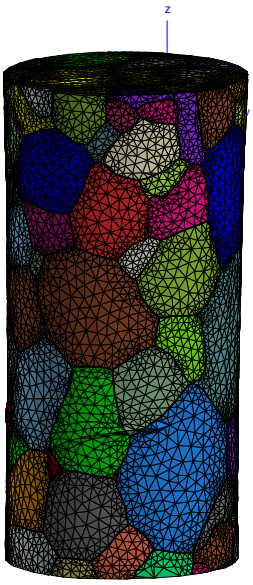

(c) Full 3D mesh ready for FEM computation

Fig. 10: Generation of a 3d mesh from a reconstructed sample imaged with DCT.

and a sharp discontinuity can be stated as producing an appropriate spatial discretization of such a problem with a reasonable number of elements. Fortunately, solutions to this problem are becoming more and more available: one may benefit at the same time of (i) the general increase in computational power, (ii) using of parallel computing and (iii) using more powerful remeshing and topological simplification algorithms. It is important to highlight that this particular cracking problem is made far more complex by segmentation errors which may produce holes and/or unwanted features in the crack geometry.

Inserting a 3D mesh of a crack imaged by microtomography into a grain network is still a challenge. A simple example with an ideal crack geometry is showed on Fig. 11 for illustration purpose. A flat penny shape crack has been inserted into the β titanium microstructure studied previously. The grain topology has been perfectly preserved and the mesh is refined around the crack to capture the expected stress concentration.

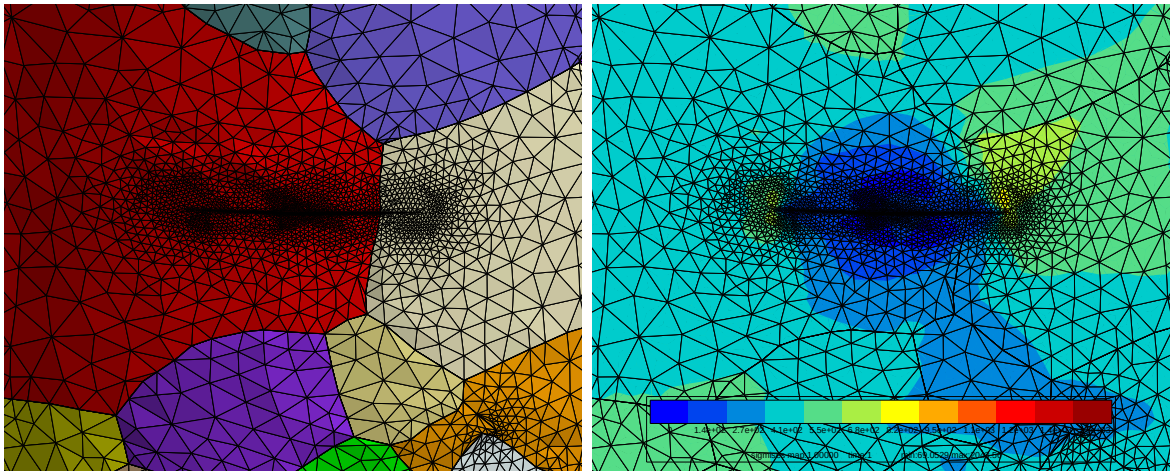

(a) Close up view of the crack inserted within the grain microstructure

(b) von Mises stress after applying 150 N tension load

Fig. 11: FE computation after inserting a crack into the polycrystalline sample.

3D crack computations based on the real grain geometry and orientations are very promising to predict the stress/strain development ahead of the crack tip. This will allow to pin down why linear fracture mechanics breaks down at this scale and what kind of models (cohesive zones, damaging elements or even coupling with discrete dislocations) can account for the short crack behaviour.

6. CONCLUSIONS AND PROSPECTS

This paper first showed how large scale finite element simulations of polycrystalline aggregates have become a standard way to study the heterogeneous deformation of materials. It was shown how to properly define a polycrystal representative volume element and how the 3D grain shape may influence the strain heterogeneities development.

Aside general computations used to assess the homogenised behaviour of a polycrystal, large scale crystal plasticity computations are now ready to simulate complete specimens based on the real grain geometries and shapes. A numerical avatar of the sample can be quite easily obtained for thin films with a columnar grain geometry but can also be retrieved

for the general 3D case thanks to recent advances using diffraction contrast tomography. Closing the gap between 3D experimental techniques able to probe strains at the grain level and below and computational mechanics is the key to extensively test the many micro-mechanical models available in the literature. This may lead to significant advances in closely related problems such as the propagation of microstructurally short cracks in a grain network.

REFERENCES

Aifantis, E. (1987). The physics of plastic deformation. International Journal of Plasticity, 3:211–248.

Barbe, F., Decker, L., Jeulin, D., and Cailletaud, G. (2001a). Intergranular and intragranular behavior of polycrystalline aggregates. part 1: F.e. model. International Journal of Plasticity, 17:513–536.

Barbe, F., Forest, S., and Cailletaud, G. (2001b). Intergranular and intragranular behavior of polycrystalline aggregates. part 2: Results. International Journal of Plasticity, 17(4):537–563.

Barbe, F., Quey, R., Musienko, A., and Cailletaud, G. (2009). Three-dimensional characterization of strain localization bands in high-resolution elastoplastic polycrystals. Mechanics Research Communications, 36:762–768.

Cailletaud, G., Forest, S., Jeulin, D., Feyel, F., Galliet, I., Mounoury, V., and Quilici, S. (2003). Some elements of microstructural mechanics. Computational Materials Science, 27(3):351–374.

Déprés, C., Robertson, C., and Fivel, M. (2004). Crack initiation in fatigue: experiments and three–dimensional dislocation simulations. Materials Science and Engineering, A387–389:288–291.

Diard, O., Leclercq, S., Rousselier, G., and Cailletaud, G. (2005). Evaluation of finite element based analysis of 3d multicrystalline aggregates plasticity application to crystal plasticity model identification and the study of stress and strain fields near grain boundaries. International Journal of Plasticity, 21(4):691–722.

El Houdaigui, F., Forest, S., Gourgues, A.-F., and Jeulin, D. (2007). On the size of the representative volume element for isotropic elastic polycrystalline copper. In Y. Bai, Q. Z. and Wei, Y., editors, IUTAM Symposium on Mechanical Behavior and Micro-Mechanics of Nanostructured Materials, pages 171–180, Beijing, China. Springer.

Ferrié, E., Buffière, J.-Y., Ludwig, W., Gravouil, A., and Edwards, L. (2006). Fatigue crack propagation: In situ visualization using X-ray microtomography and 3D simulation using the extended finite element method. Acta Materialia, 54(4):1111–1122.

Feyel, F. (1999). Multiscale FE^2 elastoviscoplastic analysis of composite structures. Computational Materials Science, 16:344–354.

Flouriot, S., Forest, S., and Remy, L. (2003). Strain localization phenomena under cyclic loading: Application to fatigue of single crystals. Computational Materials Science, 26(SUPPL.):61–70.

Forest, S. (2008). Some links between cosserat, strain gradient crystal plasticity and the statistical theory of dislocations. Philosophical Magazine, 88:3549–3563.

Frigo, M. and Johnson, S. G. (2005). The design and implementation of FFTW3. Proceedings of the IEEE, 93(2):216–231. Special issue on "Program Generation, Optimization, and Platform Adaptation".

Gairola, B. and Kröner, E. (1981). A simple formula for calculating the bounds and the self–consistent value of the shear modulus of polycrystalline aggregates of cubic crystals. Int. Engng Sci., 19:865–869.

Héripré, E., Dexet, M., Crépin, J., Gélébart, L., Roos, A., Bornert, M., and Caldemaison, D. (2007). Coupling between experimental measurements and polycrystal finite element calculations for micromechanical study of metallic materials. International Journal of Plasticity, 23(9):1512–1539.

Huet, C. (1990). Application of variational concepts to size effects in elastic heterogeneous bodies. J. Mech. Phys. Solids, 38:813–841.

Kanit, T., Forest, S., Galliet, I., Mounoury, V., and Jeulin, D. (2003). Determination of the size of the representative volume element for random composites : statistical and numerical approach. International Journal of Solids and Structures, 40:3647–3679.

Ludwig, W., King, A., Reischig, P., Herbig, M., Lauridsen, E., Schmidt, S., Proudhon, H., Forest, S., Cloetens, P., du Roscoat, S. R., Buffière, J., Marrow, T., and Poulsen, H. (2009a). New opportunities for 3d materials science of polycrystalline materials at the micrometre lengthscale by combined use of x-ray diffraction and x-ray imaging. Materials Science and Engineering: A, 524(1-2):69–76. Special Topic Section: Probing strains and Dislocation Gradients with diffraction.

Ludwig, W., Reischig, P., King, A., Herbig, M., Lauridsen, E., Johnson, G., Marrow, T., and J.Y., B. (2009b). Three-dimensional grain mapping by x-ray diffraction contrast tomography and the use of friedel pairs in diffraction data analysis. Review of Scientific Instruments, 80(3).

Musienko, A. and Cailletaud, G. (2009). Simulation of inter- and transgranular crack propagation in polycrystalline aggregates due to stress corrosion cracking. Acta Materialia, 57:3840–3855.

Neighbours, J. R. and Alers, G. A. (1958). Elastic constants of silver and gold. Phys. Rev., 111(3):707–712.

Nygårds, M. (2003). Number of grains necessary to homogenize elastic materials with cubic symmetry. Mechanics of Materials, 35:1049–1057.

Parisot, R., Forest, S., Gourgues, A., Pineau, A., and Mareuse, D. (2001). Modeling the mechanical behavior of a multicrystalline zinc coating on a hot-dip galvanized steel sheet. Computational Materials Science, 19:189–204.

Pfeifer, M. A., Williams, G. J., Vartanyants, I. A., Harder, R., and Robinson, I. K. (2006). Three-dimensional mapping of a deformation field inside a nanocrystal. Nature, 442(7098):63–66.

Poulsen, H. F. (2004). Three-Dimensional X-ray Diffraction Microscopy– Mapping Polycrystals and Their Dynamics, volume 205 of Springer Tracts in Modern Physics. Springer, Berlin.

Sanchez-Palencia, E. and Zaoui, A. (1987). Homogenization techniques for composite media. Lecture Notes in Physics No. 272, Springer, Berlin.

Šiška, F., Weygand, D., Forest, S., and Gumbsch, P. (2009). Comparison of mechanical behaviour of thin film simulated by discrete dislocation dynamics and continuum crystal plasticity. Computational Materials Science, 45:793–799.

Takagi, S. (1969). A dynamical theory of diffraction for a distorted crystal. Journal of the Physical Society of Japan, 26(5):1239–1253.

Teodosiu, C. (1997). Large plastic deformation of crystalline aggregates. CISM Courses and Lectures No. 376, Udine, Springer Verlag, Berlin.

Teodosiu, C., Raphanel, J., and Tabourot, L. (1993). Finite element simulation of the large elastoplastic deformation of multi-crystals. In Teodosiu, C. and Sidoroff, F., editors, Large Plastic Deformations MECAMAT'91, pages 153–158. Balkema, Rotterdam.

Vaxelaire, N., Proudhon, H., Labat, S., Kirchlechner, C., Keckes, J., Jacques, V., Ravy, S., Forest, S., and Thomas, O. (2010). Methodology for studying strain inhomogeneities in polycrystalline thin films during in situ thermal loading using coherent x-ray diffraction. New Journal of Physics, 12(3):035018.

Šiška, F., Forest, S., and Gumbsch, P. (2007a). Simulation of stress–strain heterogeneities in copper thin films: Texture and substrate effects. Computational Materials Science, 39:137–141.

Šiška, F., Forest, S., Gumbsch, P., and Weygand, D. (2007b). Finite element simulations of the cyclic elastoplastic behaviour of copper thin films. Modelling and Simulation in Materials Science and Engineering, 15(1):S217–S238.

Zeghadi, A., Forest, S., Gourgues, A.-F., and Bouaziz, O. (2007a). Ensemble averaging stress–strain fields in polycrystalline aggregates with a constrained surface microstructure–Part 2: Crystal plasticity. Philosophical Magazine, 87(8-9):1425–1446.

Zeghadi, A., N'Guyen, F., Forest, S., Gourgues, A.-F., and Bouaziz, O. (2007b). Ensemble averaging stress–strain fields in polycrystalline aggregates with a constrained surface microstructure–Part 1: Anisotropic elastic behaviour. Philosophical Magazine, 87(8-9):1401–1424.